Surface patterning of low-dimensional systems: the chirality of charged fibres

2009 J. Phys.: Condens. Matter 21 424114

(http://iopscience.iop.org/0953-8984/21/42/424114)

J. Phys.: Condens. Matter **21** (2009) 424114 (10pp) doi:10.1088/0953-8984/21/42/424114

Surface patterning of low-dimensional systems: the chirality of charged fibres

K L Kohlstedt[1,2], G Vernizzi[2] and M Olvera de la Cruz[1,2]

[1] Department of Chemical and Biological Engineering, Northwestern University, Evanston, IL 60208, USA
[2] Department of Materials Science and Engineering, Northwestern University, Evanston, IL 60208, USA

E-mail: m-olvera@northwestern.edu

Received 30 March 2009, in final form 27 April 2009
Published 29 September 2009
Online at stacks.iop.org/JPhysCM/21/424114

Abstract
Charged surfaces are interesting for their ability to have long-range correlations and their ability to be dynamically tuned. While the configurations of charged planar surfaces have been thoroughly mapped and studied, charged cylindrical surfaces show novel features. The surface patterning of cylindrically confined charges is discussed with emphasis on the role of chiral configurations. The origins of surface patterns due to competing interactions in charged monolayers are summarized along with their associated theoretical models. The electrostatically induced patterns described in this paper are important in many low-dimensional biological systems such as plasma membrane organization, filamentous virus capsid structure or microtubule interactions. A simple model effectively predicting some features of chiral patterns in biological systems is presented. We extend our model from helical lamellar patterns to elliptical patterns to consider asymmetrical patterns in assemblies of filamentous aggregates.

(Some figures in this article are in colour only in the electronic version)

1. Introduction

Since the middle of the twentieth century, physicists and biologists have been interested in heterogeneities on the surface of model membranes with the goal of understanding the cellular plasma membrane [1–7]. Langmuir–Blodgett films provided the initial clue that a monolayer comprised of a two-component lipid mixture showed gas–liquid order transitions [8]. With the advance of fluorescence microscopy, individual domains were visualized and the coexistence of solid, liquid and gas phases of a lipid could be visualized in real time [9–11, 3]. Interestingly, complex shaped finite size domains of size L in addition to undulating phases with lamellar and hexagonal ordering were observed [1, 9, 12–15, 2, 16, 17, 5]. The observed finite size domains in these systems have been shown to be due to competing interactions, especially short-range steric chemical mismatches and long-range dipolar interactions [18, 19]. In two dimensions long-range order is thought to be destroyed for domains interacting through a potential $\sim 1/r^m$ that decays faster than two or more generally when $m > d$ for d dimensions [20–23, 18]. However, long-range ordering of such domains or patterns (i.e. correlation length $\xi \gg L$) has been observed on interfaces such as charged membranes and surfaces [24, 25, 11, 26–28]. To be clear, in systems far below the critical temperature $T \ll T_c$ long-range order is observed independent of dimensionality (as seen in the Ising model with short-range interactions) [29, 30], but in two dimensions long-range interactions like electrostatics can lead to domain ordering due to domain repulsion even near T_c [26]. Actually, even crystalline order (not domain ordering) has *not* been excluded in two dimensions for systems that interact with an electrostatic potential $\sim 1/r$ [21].

Finite size domains are not unique to systems with competing long- and short-range interactions. Purely repulsive interactions such as ion correlations in polyelectrolytes, soft-core potentials and metastable or glassy systems have all shown the propensity to form domains on surfaces [31–37, 15, 38–40]. Ferromagnetic layers offer another possibility to see patterning [41], as well as supramolecular assemblies with multilayers having polar order [42]. Further, surface domains have been observed to not only segregate ordered and disordered molecular conformations, but also discriminate between isomeric states

such as D- and S-chiral enantiomers [43–49]. In the latter case, the line tension of the domains is asymmetric due to the interactions of the chiral molecules [48].

Electrostatic interactions have been shown to amplify the asymmetry in the line tension leading to interesting clover, chiral bananas and spiral shapes [43, 9, 50, 51]. Chiral discrimination has also been observed in quasi-one-dimensional systems with chiral promoter molecules such as the 'sergeants and soldiers' technique and 'majority rules' phenomena [52, 53]. Helical patterning of cylindrical aggregates is an example that has been studied lately due to the many biological aggregates that support helical shapes [54–58, 53, 59–65]. This paper will discuss how heterogeneously charged surfaces in quasi-one-dimensional systems could be an explanation for the ubiquitous helical symmetry seen in biomolecular assemblies. We first give an introduction to order–disorder transitions in planar assemblies, especially paying attention to charged monolayers and bilayers. We then introduce a model for describing charge patterns on the surface of cylindrical assemblies. In the final section we relate the model to predicting properties of helical assemblies of biological molecules.

1.1. Surface patterning of planar systems

Andelman *et al* [1] were the first to consider periodic patterns on the surface of a two-component lipid monolayer. Amphiphilic molecules like lipids have a polar head and carry a dipole moment. At an air/water interface the electrostatic interaction between dipoles have long-range interactions and can lead to the possibility of periodic domains [1, 12, 66–68]. Hexagonal domains generally appear when the solid phase component is less dense, while a lamellar phase occurs when the two components are equal in concentration (see figure 1) [12].

A mean-field approach was used by considering a system of liquid lipids floating in a gas state near the critical temperature [1]. Using Ginzburg–Landau theory to expand the Hamiltonian they were able to construct a phase diagram of a weakly segregated system using a single dominant wavenumber (single-mode analysis) [1]. We will now discuss the two-phase coexistence region for cationic and anionic lipids coexisting with a gas phase in the strong segregation limit. Namely, our interest lies with charged patterns at the low temperature limit where strongly segregated phases occur.

McConnell and others show a similar model as previously, but only consider the strongly segregated case (i.e. $T \ll T_c$) [12]. They find hexagonal arranged domains at more rarefied packings, while a lamellar phase exists at denser lipid packings with a phase coexistence area surrounding the lamellar phase [12]. Several experiments with chromophores attached to the lipid allowed for visual conformation of the phases [9, 69, 4, 70]. Subsequent, x-ray scattering experiments [71, 72] and numerous theoretical treatments [17] (mainly based on Landau theory) have found a much richer phase diagram, especially with orientational ordering. This leads many to believe that simple one-dimensional dipolar interactions may be freezing out further order [17, 2]. Pure

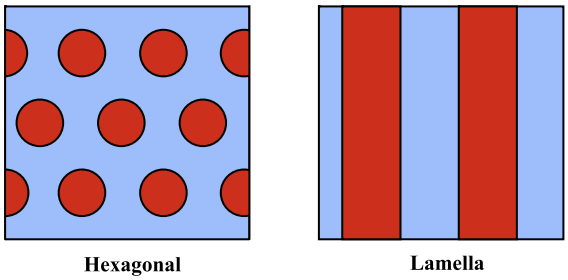

Figure 1. Periodic, undulating patterns found in planar systems with competing interactions. The size of the pattern depends on how strong the electrostatic interaction is compared to the steric mismatch of the ordered and disordered components.

Coulomb interactions provide another pathway to investigate long-range order with competing interactions.

The dipolar free energy for the striped phase proposed by Andelman *et al* [1] includes a non-specific interaction that accounts for the propensity to be in one phase over the other. A second set of terms takes into account whether the system prefers to be in the striped phase or isotropic phase [1]. Finally, the small effect (presumably at low temperatures) of a diffuse boundary between the phases is considered as a spatially dependent line tension [1, 51]. At equilibrium the lamellar phase minimizes the free energy at concentrations near stoichiometric ratios 1:1 gas phase and liquid phase lipids [1, 12].

Recently, Solis *et al* [73, 2] have written a phenomenological free energy describing a similar system in which co-assembled positive and negative charged molecules are confined to a two-dimensional surface. In this system they assume one component of the assembled surface forms a strongly segregated domain due to chemical (van der Waals) affinity between the molecules of like charge accountable by the line tension [74]. The system is assumed to have not have correlated ions bound to the surface, so dipolar interactions are not considered here [73]. Examples of such a system can be seen in weakly charged lipid bilayers [3, 75], but also ionic surfactants adsorbed onto mica, silica and graphite [76–78] or gold [79]. Weakly charged polyelectrolytes with a hydrophobic backbone adsorbed onto oppositely charged surfaces also show periodic patterning again due to the long-range nature of the electrostatic repulsion [80–83]. The model of Solis *et al* [73] begins with writing the free energy density (per area) $\Im$ of a periodic Wigner cell at low temperature, where the ordered structure has a charge that is smeared out by the disordered phase, namely

$$\Im = \frac{\gamma}{L} s_1 + \frac{\sigma L}{\varepsilon} s_2. \tag{1}$$

The parameter γ represents the line tension between the phases, with σ and ε representing the surface charge density and dielectric permittivity, respectively [73]. The parameters s_1 and s_2 describe the relationship between the Wigner cell and the periodic lattice. Specifically, s_1 represents the interfacial length of the ordered domain inside the Wigner cell and s_2 is the interaction of the domains on a lattice via the screened electrostatic interaction via a Yukawa potential. After writing

a dimensionless free energy $\Im_0 = \frac{s_1}{d} + s_2 d$ the minimization of the free energy depends only on the parameters s_1 and s_2 and the dimensionless length L/L_0, with the characteristic length $L_0 = \frac{\sqrt{\gamma\varepsilon}}{\sigma}$ [73]. The calculation of s_1 for lamellar domains is simply the number of interfaces in the Wigner cell, namely 2 (scaled by the cell size L) [84]. For the circular domains s_1 is the circumference again scaled by L. The calculation of s_2 requires a sum over the entire periodic surface as each cell interacts through the screened electrostatic potential with the expression

$$s_2 = \frac{1}{2}\sum_{\mathbf{\Lambda}} \int_{\text{cell}} \mathrm{d}\mathbf{x} \int_{\text{cell}} \mathrm{d}\mathbf{y}\sigma(\mathbf{x})\sigma(\mathbf{y})V(\mathbf{y}-\mathbf{x}+\mathbf{\Lambda}), \quad (2)$$

and $\mathbf{\Lambda}$ representing the lattice vector. The potential $V(\mathbf{x}) = \frac{\mathrm{e}^{-\kappa x}}{|\mathbf{x}|}$ is simply the standard Debye–Hückel screened electrostatic potential. After minimizing the free energy they find hexagonal domains below an area fraction $f \cong 0.34$ (and its corresponding point $f \cong 0.66$) with lamellar domains at intermediate values similar to those seen in figure 1, where f is the fraction of the ordered domain species over the total Wigner cell size [73, 84]. For this model the energy is symmetric at the point $f = 0.5$, since there is no preference for either component. The phase diagram of the hexagonal and lamellar domains is visualized in figure 2. Lamellar charged patterns are seen at intermediate values $0.34 < f < 0.66$.

The characterization of the interfaces between the gas and solid phases are considered by looking at the coexistence of ordered lamellar/hexagonal domains with a disordered gas phase. The free energy of the gas phase is comprised of a Flory–Huggins free energy density (per unit area) $\Im_G$ in equation (3) [1, 85, 86] while the solid phase electrostatic repulsion term $\Im_S$ is

$$\frac{\Im_G}{kT} = \frac{1}{N}\Phi\log\Phi + \left(\frac{1}{a_0} - \Phi\right)\log\left(\frac{1}{a_0} - \Phi\right) + \chi\Phi(1-\Phi a_0) \quad (3)$$

$$\Im_S = -\frac{1}{4\pi}\int \phi(\mathbf{r})g(|\mathbf{r}-\mathbf{r}'|)\phi(\mathbf{r}')\,\mathrm{d}^2\mathbf{r}\,\mathrm{d}^2\mathbf{r}'$$
$$g(\mathbf{r}) \propto \left(\frac{1}{\varepsilon\,(\varepsilon+\varepsilon_0)}\right)\frac{1}{\mathbf{r}^\alpha}, \quad (4)$$

with Φ being the total concentration of the monolayer, N is the number of charges in the gas phase and a_0 is the area per head group. In equation (4) the solid phase concentration is ϕ, while ε and ε_0 are the permittivity in the dielectric and free space, respectively. The decay of the repulsive power law potential $g(\mathbf{r})$ in the solid phase can be $\alpha = 1$ for Coulomb and $\alpha = 3$ for dipolar and the enthalpic immiscibility is $\chi > 0$. It is clear that the partition function does not account for any order due to the molecular details of the components as (1) the Flory–Huggins description does not account for those structural details and (2) the population N does discriminate between gas phase direction in the plane of the interface and perpendicular to the interface in the ordered phase. The free energies for the isotropic, hexagonal and striped phases are all expanded around the critical point and minimized under the constraint $\Im_i - \mu\Phi_0$, where i represents one of the three phases and μ is the Lagrange multiplier (in this case the chemical potential) Φ_0 is the reduced concentration. An example for a dipolar field (instead of electrostatic) can be seen in a phase diagram (not reproduced here) that has five phases in contact at the critical point: a hexagonal, a lamellar and an inverted hexagonal phase along with a liquid and gaseous phase [1]. This highlights the result that electrostatic interactions (as well as dipolar) are able to stabilize periodic patterns on a two-dimensional monolayer. We note that in three dimensions electrostatics do stabilize finite-sized domains, while dipolar interactions do not.

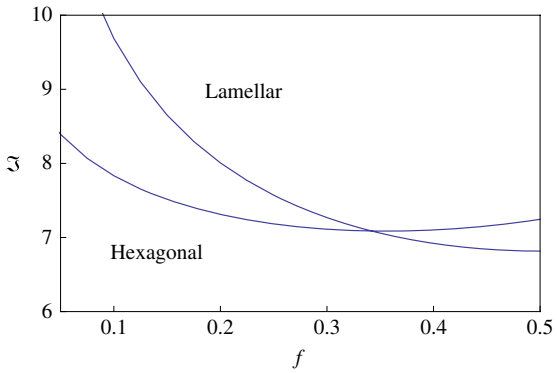

Figure 2. Phase diagram of a planar two-component charged system with hexagonal and striped (lamellar) domains possible. The free energy $\Im$ (shown in equations (1)) is plotted versus the area fraction f of one of the charge components. The diagram is cut at its symmetric point in the area fraction. The transition occurs at $f = 0.34$. Adapted with permission from [73]. Copyright 2005 by the American Institute of Physics.

Finally, we end the discussion on planar systems with recent work done by Loverde *et al* [86, 87]. The coexistence of two possible phases at low temperature was considered. One phase consists of a dense, patterned solid formed by the oppositely charged components. Its free energy can be computed by assuming the formation of regions of constant particle and charge density similar to equation (1) [73, 86]. The second phase is homogeneous gaseous state and has a low density of charged particles. It was treated as a two-dimensional charged gas in a homogeneous background that displays non-selective interactions with the charged components and its free energy is f_G (equation (3)). The free energy of the low density homogeneous gas of charged particles can be calculated using linear response theory by means of the one-loop approximation or random phase approximation (RPA) at the interface [88]. Using the ESPResSO simulation package to perform NVT simulations [89, 86], the interface of the positive and negative domains in the two-phase coexistence was investigated.

For asymmetric charge ratios of charge valency, figure 3(a) shows the formation of a hexagonally patterned 'island' at densities $\rho = 0.10$ [86]. For higher densities, as in figure 3(b), the solid phase occupies a larger fraction of the space but exhibits a more clearly ordered structure. For symmetric charge ratios, the ordering is lamellar [86]. At higher values (figure 3(d)), the interfaces are much sharper and exhibit smaller interfacial fluctuations [86]. The orientation of the lamellar may be due to the minimization of the local

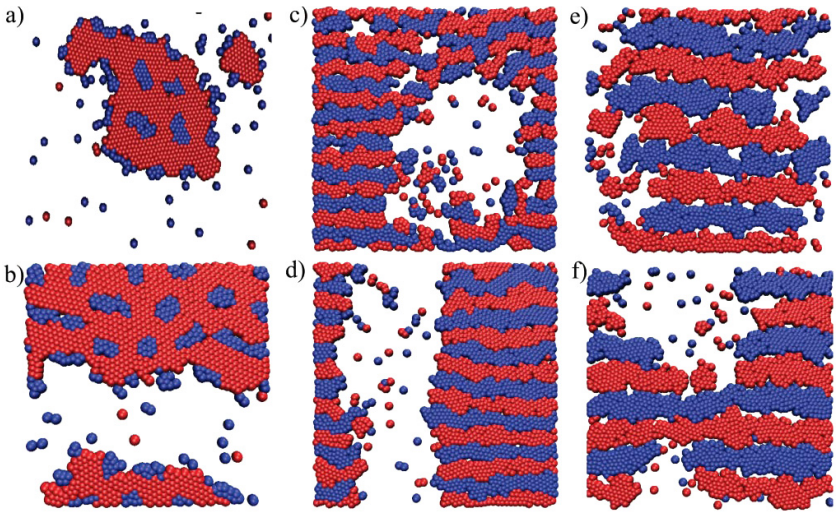

Figure 3. Coexistence of solid and gas phases in a two-dimensional monolayer of positively (red) and negatively (blue) charged spheres. When rich in positive charges near a ratio of 3:1, hexagonal domains form (a) and (b), while for symmetric charge ratios 1:1 lamellar domains form (c)–(f). Closer to the order to disorder transition a clear coexistence is observed. Reproduced with permission from [86]. Copyright 2007 by the American Physical Society.

electrostatic energy. Figures 3(e) and (f) show the transition from a solid to a solid–gas coexistence phase for symmetric charge ratios but for weaker electrostatic interactions [86]. At low values of the cohesive energy ε, the system shows the lamellar patterning but possesses large voids between the charged domains, effectively reducing the line tension between domains. The strong segregation theory in equation (1) gives a characteristic length that scales with the ratio of short-range interactions over long-range interactions with an exponent of $\eta = 1/2$ in two dimensions and $\eta = 1/3$ in three dimensions [73]. Good agreement is found from simulations (in two dimensions) with a scaling of $\eta \cong 0.47$ [86, 40]. Better agreement could be found if the strong segregation theory included the reduction in line tension due to the defects forming along the lamellar. A good treatment of fluctuations in order/disorder transitions can be seen in the work of Levin and Dawson [90], as well as Olvera de la Cruz [91]. It is possible that density fluctuations can renormalize the line tension and lead to complex phase diagrams [92, 93]. From a technological point of view, domains with charge segregation have been shown to be critical in polymer matrix photovoltaic sheets [94]. To reiterate, dipolar and higher multipolar interactions [95, 96] do not have long-range ordering ability in three dimensions while electrostatic do show finite domains [97], which can be seen in the decay of the three-dimensional static structure factor $\sim 1/k^2$ [21].

1.2. Ionic patterning of cylindrical assemblies

From a theoretical vantage point, the electrostatic patterning of a system of charges on low-dimensional surfaces ($1 < d < 2$) such as cylindrical surfaces is relatively unexplored. Certainly, the effects of long-range electrostatic forces have been widely studied for planar two-dimensional systems as outlined above; also the behaviour of short-range interactions over cylindrical geometries has been addressed, such as the Ising model with surface curvature like the cylinder [98]. Similar to the above we are interested here in summarizing work done on surface charge patterning on cylinders. Interestingly, charge patterning on cylindrical surfaces includes many structures in biology, especially in the extracellular membrane (see the next section). However, there is also recent work that proposes surface structure is due not to the long-range nature of electrostatic interactions, but due to mulitpolar interactions causing anisotropic interactions through direction-specific packing, especially with regard to helical patterning [95]. In this work they use a Monte Carlo simulation to competitively self-assemble a system of particles with van der Waals interactions against dipolar, quadrupolar and hexapolar interactions in a bulk fluid state. Using a seeding mechanism to influence the energy surface they find complex structures such as chains, loops, nanotubes and membranes [95, 99].

They conclude with the observation that symmetric ionic fluids prefer to form square quadrupoles, while asymmetric ones prefer dipoles and linear quadrupoles and therefore form chains while the former tend to make sheets and tubes [95]. Further, hexapoles were shown to favour icosahedral formation similar to viral capsid shells [95], a separate work that has been of interest to us [100].

A case is analysed here where charges are confined over a cylindrical surface and interact via electrostatic interactions [64]. Further, it is examined whether spherically symmetric electrostatic interactions are capable of breaking the chiral isometry of the cylinder. Recently, there has been interest in the study of crystalline systems over constrained geometries such as the surface of spheres, cylinders and tori [101–104].

The generalization to more general curved substrates shows an interesting rich behaviour [61, 76]. A model is generalized from Solis *et al* [73] for charge domains on cylindrical cationic–anionic co-assemblies. A 1:1 stoichiometric mixture that covers the surface completely

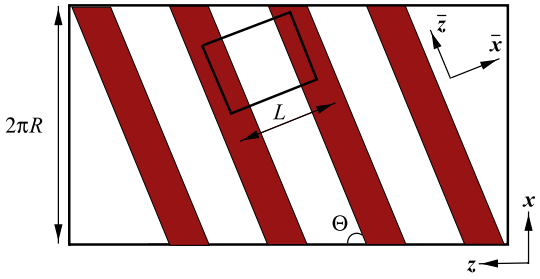

Figure 4. Lamellar patterns tiled on unwrapped cylinder. The definition of the periodic cell (outlined box) with characteristic cell size L is shown. The pitch angle Θ of the striped domains is shown with respect to the axis of the cylinder. Redrawn with permission from [64]. Copyright 2007 by the American Physical Society.

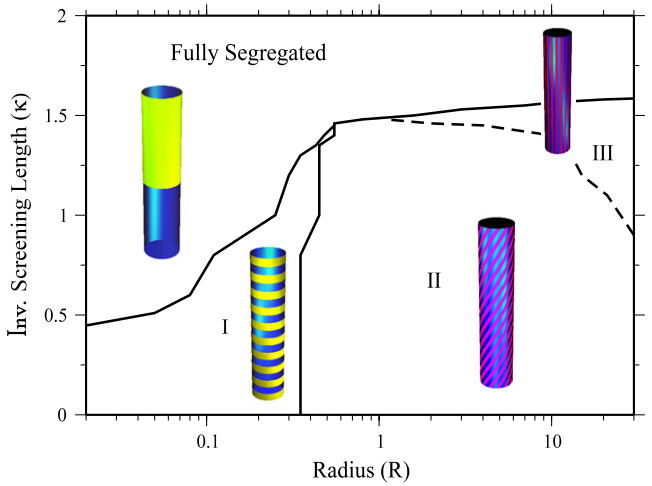

Figure 5. Phase diagram of striped patterns confined on a cylindrical fibre in the space of cylinder size R and electrostatic interaction distance κ. Three phases are observed that have a finite cell size along with a macroscopically segregated phase. Redrawn with permission from [64]. Copyright 2007 by the American Physical Society.

is considered. Lamellar domains have been predicted and observed under similar conditions [73, 12, 1] and we begin by focusing on striped patterns. Similar to [73, 1] an incompatibility χ between unlike charges results in a line tension γ that forms between the domains rich in one component. Molecules of like charge form homogeneous domains of average charge density σ. This model assumes the system is far from T_c and well within the strongly segregated limit and the corresponding lowest energy configuration is domains arranged on a periodic lattice $\{\Lambda\}$.

The free energy density F over a cell is considered with a cell area A_c being the area of the Wigner–Seitz cell [18]. The system is described by a two-term phenomenological free energy similar to equation (1), where $F = F_1 + F_2$ with F_1 the short-range line tension term and F_2 the long-range electrostatic term. We take F_0 to be the dimensionless free energy similar to $\Im_0$ by scaling by the characteristic length $L_0 = \frac{\sqrt{\gamma\varepsilon}}{\sigma}$ and measuring the free energy in terms of dimensionless units. In this case, $F_1 = 2/L$ where L is the distance between two neighbouring lamellae. F_2 can be computed first by 'unwrapping' the surface of the cylinder of radius R onto an infinite set of parallel stripes of size $2\pi R$ on the plane and then by summing all the pairwise screened electrostatic interactions $V(\mathbf{x})$ over the planar periodic lattice of the lamellae. To simplify the calculations we adopted a square lattice oriented along the lamellae shown in figure 4. Formally:

$$F_2 = \tfrac{1}{2}\sum_{\Lambda}\int_{\text{cell}} \mathrm{d}\xi \int_{\text{cell}} \mathrm{d}\eta\sigma(\xi)\sigma(\Lambda+\eta) \times V(\Lambda+\eta-\xi), \tag{5}$$

where

$$V(\mathbf{p}) = \frac{\mathrm{e}^{-\kappa D}}{4\pi D}\theta(2\pi R - |p_x|), \tag{6}$$

with $D \equiv \sqrt{4R^2\sin^2\frac{p_x}{2R} + p_z^2}$ being the projected distance of $\mathbf{p} = (p_x, p_z)$ on the $\{x, z\}$ plane and $\theta(x)$ is the step function. By introducing the reciprocal lattice $\mathbf{Q}$, defined by $Q\cdot\Lambda = 2\pi m$, and by using the Poisson summation formula we have [64]

$$F_2 = \frac{1}{2A_c}\sum_{\mathbf{Q}}\hat{\sigma}(\mathbf{Q})\hat{\sigma}(-\mathbf{Q})\hat{V}(\mathbf{Q}), \tag{7}$$

where $\hat{\sigma}(\mathbf{Q})$ and $\hat{V}(\mathbf{Q})$ are the Fourier transforms of σ and V, respectively. They are

$$\hat{\sigma}(\mathbf{Q}) = 4\frac{\sin(\bar{q}_x/4)}{\bar{q}_x}\delta(\bar{q}_z), \tag{8}$$

$$\hat{V}(\mathbf{Q}) = RI_{q_xR}(\xi)K_{q_xR}(\xi), \tag{9}$$

where $\xi = R\sqrt{\kappa^2+q_z^2}$, and I_v and K_v are modified Bessel functions of order of the first kind and second kind, respectively [64]. For simplicity we used the twofold notation $\mathbf{Q} = (q_x, q_z)$ in the reference system parallel to the lamellar domains and $\mathbf{Q} = (\bar{q}_x, \bar{q}_z)$ in the reference system parallel to the axis of the cylinder (see figure 4) [64]. Let Θ be the pitch angle between the axis of the cylinder z and the direction of the lamellar stripes. Any lattice on the surface of a cylinder must be commensurate with its circumference or it must be periodic in the x direction with period $2\pi R$. The commensurability constraint in the reciprocal space is $\bar{q}_x = 2\pi m/L$ or equivalently $q_x = 2\pi m\cos\Theta/L$ and $q_z = 2\pi m\sin\Theta/L$. Moreover $q_xR = mn$ must hold, where n is the number of lamellar stripes per pitch [64]. The free energy density F is numerically minimized with respect to all possible lamellar lattices, i.e. with respect to the spacing L and the pitch angle Θ for several values of R and κ.

The results are contained in a phase diagram in the space of κ and R in figure 5. The phase diagram shows three periodic phases and a macroscopically segregated phase. Phase **I** is located at $R \ll L$ where the circumference is smaller than the domain size. This is a degenerate phase where $q_x = 0$ and the rings stack up the length of the cylinder. Phase II is the helical phase that surprisingly assumes chiral symmetry. The electrostatic interactions are presumed to be the reason the phase prefers to adopt chiral symmetry, due to increasing κ leads to a continuous transition to a non-helical phase **III** vertical lamellar domain. Further, the asymptotic

expansion of the free energy shows asymmetry in the second-order term and minimization with respect to Θ at $\kappa = 0$ gives $\Theta^* = \arccos\sqrt{\frac{3}{5}}$. This value is within numerical precision of what the helical pitch Θ is found to be in phase **II** at $\kappa = 0$. This angle is found to be preserved over a wide range of radii.

Interestingly, the helical phase is stabilized only in the case of the $\sim 1/r$ potentials as, when dipolar interactions $\sim 1/r^3$ are considered, only vertically striped periodic patterns are stabilized. Higher-order multipolar terms show the same behaviour. This shows that the interplay of the Coulomb potential with the striped phase on the cylinder uniquely gives rise to chiral symmetry [64]. Further, the investigation of other types of patterns such as circular domains reveals a preference for achiral configurations on the cylinder. Similarly, an fcc ionic lattice wrapped around a cylinder showed a similar trend, although a tethered ionic lattice has led to interesting trapped states [105]. Finally, upon elongation of circular charged domains into highly asymmetrical elliptical domains with eccentricities less than ~0.75, the lowest energy configuration returns back to helical wrappings showing that, as the circular pattern transforms into a lamellar-like pattern, chiral symmetry is preferred (see subsequent section) [105].

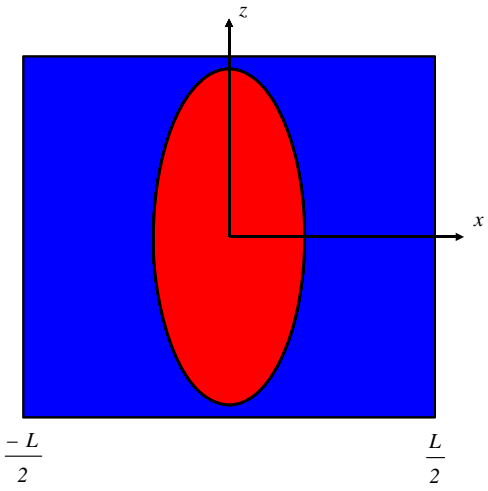

Figure 6. Schematic of elliptical domain in a periodic cell size L. The positively charged domain is in the interior of the ellipse (red) while the negatively charged domain surrounds (blue). At high asymmetries the phase diagram of the elliptical domain behaves similar to that of the lamellar domain (shown), while ellipses similar to a circular domain remain isotropic.

2. Self-assembled biological fibres

We have discussed in section 1 that a significant thrust of the past 25 years has been in the area of understanding the composition and ordering of the plasma membrane [6, 3, 4]. The much debated surface patterning of cell membranes or 'lipid rafts' has shown promise in model vesicles, but has no clear evidence in cellular membranes [106]. A less well-studied, but related area, is membrane interacting filaments such as filamentous viruses and microfilaments surrounding the cell membrane [59, 107–110]. Additionally, filamentous viruses have a helical capsid that surrounds the genome [109, 107]. In this section, a brief summary is given of the recent work that describes lamellar patterns on assembled biological fibres, especially those with helical arrangements [111]. The subsequent section will show a comparison of an electrostatic model prediction's with that of some recent structural experiments such as NMR and x-ray diffraction.

Helical assemblies are ubiquitous in biological systems and have rightly been studied in part due to the fact that a helix has a sense of direction over many length scales—in other words it has the ability to break chiral symmetry [112–114]. Assemblies comprised of chiral components have been well categorized and efforts have been mostly focused on shifting a normally racemic mixture to one that is stereochemically pure or optically active [52]. Self-assembled systems from achiral components into chiral assemblies have had recent attention especially in the area of colloids [57, 115, 116, 63, 117]. In these systems the handedness of chirality cannot yet be controlled without explicitly breaking the symmetry [116]. The intermolecular forces responsible for giving rise to helical arrangements are still open to debate [63, 64]. In the area of colloid self-assembly, chiral arrangements have been predicted by Pickett *et al* in one-dimensional confinement of spheres arising exclusively from excluded volume constraints [63]. Since then a variety of systems from magnetically active ferrofluid capped silica colloids [57] to gold nanowires [118] have shown the ability to have chiral states. A closer look at the magnetically assembled colloids reveals the formation of the dimer that leads to chiral chains [57]. This mechanism may provide a pathway for the self-assembly of filamentous chiral aggregates similar to tubulin, which form nanotubes in the presence of GTP with helical surface arrangements and are also dimers [119, 120].

The model presented here describes a 1:1 stoichiometric mixture of oppositely charged domains that fully cover the surface of a cylinder, as described above [64]. Once again the lowest energy configuration is taken to be stripes of alternate positive and negative lamellar domains. In order to get a closer look at the electrostatic contributions to the phase diagram of lamellas on a cylinder and to describe fixed molecular arrangements discussed above [59, 110] the stripe distance L is assumed to be a fixed length. A simple order-of-magnitude analysis of the strength of electrostatic interactions in aqueous solution indicates that the typical stripe width L is at the nanometre scale. Additionally, if the radius R of the cylinder is fixed, then the only degree of freedom is the pitch angle Θ between the lamellar domains and the cylinder axis. In this case the energy function does not need to be minimized with respect to L, since L is assumed to be a fixed quantity (see figure 6). Essentially, in equation (1) the line tension is neglected and therefore the electrostatic interaction in equation (2) is minimized with respect to the pitch angle Θ. The minimization of equation (2) is not shown (see [111] for details), but the focus below is on the predictive capabilities of the model for some of the helical systems described above. The dimensionless radius $\tilde{R} = R/L$ is used in the following calculations for convenience.

The first example is a system composed of Lanreotide octapeptides self-assembled into nanotubes [59]. Then the nanotube structure is a bilayer of amphiphilic β-sheet stacked molecules that shows viral capsid-like dimensions. The Lanreotide molecules have an effective charge of $+2$ and have a radius $R = 12.2$ nm and lamellar spacing $L = 2.07 \times \sin 119^\circ = 1.81$ nm, in aqueous solution with acetate salt. Those values, plus the fact that the bilayer has a thickness of $d = 1.8$ nm, correspond to a dimensionless cylinder radius $\tilde{R} = 6.24$. The minimization of equation (2) at such a value of $\tilde{R}$ falls in the region $n = 30$ [111]. This value of n corresponds to the number of units of Lanreotides per pitch, i.e. the number of helices in a single turn, and the resulting predicted value of the pitch angle is $\Theta = 40.1^\circ$ [111]. These values are not far from the x-ray diffraction measurements of subunits of Lanreotide per pitch $n = 26$ and a pitch angle of $\Theta = 48.5^\circ$ [59].

From the x-ray measurements the authors propose a unit cell that is a stretched square lattice with lattice vectors $\{\mathbf{i} = 207$ nm, $\mathbf{j} = 208$ nm$\}$ with $\mathbf{i}$ perpendicular to the bond axis and $\mathbf{j}$ along the hydrogen bond [59]. We now extend the lamellar model [111] to include the subtleties of the above monoclinic lattice by computing a free energy for charged elliptical domains tiled around a fibre.

Asymmetric domain formation is seen in many systems with hydrogen bonding or sterically stacked molecules that align along a preferential direction (i.e. along the axis of the fibre, shown in figure 7) [121, 122]. We consider an elliptical domain tiled periodically over the surface of the cylinder. We write the charge density σ of the domain as

$$\sigma(p_x, p_z) = \begin{cases} +\bar{\sigma} & \text{for } 1 \geqslant \frac{p_x^2}{l_x^2} + \frac{p_z^2}{l_z^2} \\ -\bar{\sigma} & \text{for } 1 < \frac{p_x^2}{l_x^2} + \frac{p_z^2}{l_z^2}, \end{cases} \tag{10}$$

where $\bar{\sigma}$ is the charged density inside the elliptic domain and the stoichiometric ratio of charges is 1:1, in other words, we fix $f = 1/2$ such that we stay within the lamellar phase shown in figure 2. We again transform the density into the reciprocal lattice to make the calculation tractable by the Fourier decomposition method. The Fourier transform of σ is defined as

$$\hat{\sigma}(\mathbf{q}) = \int_{\frac{-L}{2}}^{\frac{L}{2}} \mathrm{d}x \int_{\frac{-L}{2}}^{\frac{L}{2}} \mathrm{d}z\, \sigma(\mathbf{p}) \mathrm{e}^{\mathbf{i}\mathbf{p}\cdot\mathbf{q}}, \tag{11}$$

with $\hat{\sigma}$ representing the Fourier transform of the density. The integral can be solved analytically over the domain of the cell as

$$\hat{\sigma}(q_x, q_z) = \frac{4\pi l_x l_z \bar{\sigma}}{\sqrt{q_x^2 l_x^2 + q_z^2 l_z^2}} J_1\left(\sqrt{q_x^2 l_x^2 + q_z^2 l_z^2}\right) - 4\bar{\sigma} \frac{\sin\left(\frac{q_x L}{2}\right)}{q_x} \frac{\sin\left(\frac{q_z L}{2}\right)}{q_z}. \tag{12}$$

To keep the cell electroneutral, the area of the positive charge density must be equal to the area of the negative charge density or $L^2/2 = \pi l_x l_z$. We also constrain $l_x, l_z \leqslant \frac{L}{2}$ such that the major axis of the ellipse is never larger than the cell size L.

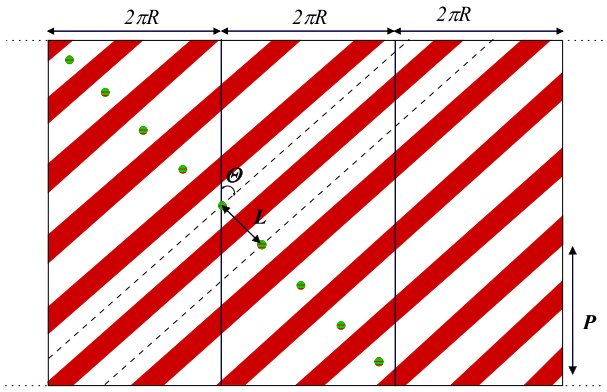

Figure 7. Charged lamellar stripes on a periodic plane of unwrapped cylinders with circumference $2\pi R$. The separation of the helices is given by L, with the pitch of a helix given by P. The helices make a pitch angle Θ with respect to the axial direction of the cylinder. Redrawn with permission from [111]. Copyright 2009 by RSC Publishing.

We calculate the free energy of the elliptical cell using the Poisson summation method described by equation (7) in section 1.2. Instead of summing over the one-dimensional lattice $\{\mathbf{\Lambda}\}$ used in the previous lamellar case, we consider a square lattice $\mathbf{\Lambda} = m\mathbf{a} + n\mathbf{b}$ of elliptical domains where (m, n) are the lattice indices and $\mathbf{a}$, $\mathbf{b}$ are the lattice vectors. A square lattice is considered here because we are interested in the highly asymmetrical limit where the square lattice of elliptical domains is approaching the lamellar lattice. We calculate the free energy density F for the lattice and look for the minimum in the pitch angle Θ. In order to determine whether chiral lattices are favoured over achiral lattices we compare fibres with equal radii that have degenerate chiral and achiral lattices associated with them. Using the ratio $r = l_x/l_z$ as a measure of the eccentricity we find that circular domains prefer achiral lattices $\Theta = 0$ or $\Theta = \pi/4$. For highly asymmetric ellipses, where $l_x = 1/\pi$ and $l_z = 1/2$ we find chiral domains for $r \lesssim 0.71$.

The above parameters from the octapeptide nanotube are now used in the elliptical model and we find better agreement with the diffraction data in describing the chiral surface structure. Using the lattice indices $m = 13$, $n = 26$ given by the x-ray data we find a pitch angle of 45° (the achiral degenerate lattice is the lowest energy state, hence $\Theta = 45^\circ$) and this value is remarkably similar to the 48.5° reported earlier [59].

A second experimental system considered is the capsid structure of the filamentous bacteriophage (Inovirus) in the Ff group (fd, $f1$ and $M13$) [107–109]. This capsid surface for this group of phages has been studied extensively with solid-state NMR [123, 109] and x-ray diffraction [124, 108]. In part because the capsid surface of the phage has been well characterized, it has been quite useful for understanding molecular chirality, especially in cholesteric liquid crystal systems [107, 112, 125, 126]. The fd virion presents a helical arrangement with a fivefold symmetry around the fibre axis, a radius of the virion $R = 2.68$ nm, a pitch distance for one helix $P = 3.3$ nm and a pitch angle $\Theta = 49^\circ$ for the similar $M13$

virus. The $M13$ virion differs from the fd by the substitution of a aspartic acid (D), which is negatively charged at biological pH, with a polar asparagine (N) at the N-terminus of the 50-residue coat protein [108]. The relation between the repeat distance of n helices or pitch and the lamellar periodicity L can be easily solved by using a bit of trigonometry from figure 7. The relation is

$$L = \frac{2\pi R P}{n\sqrt{P^2 + (2\pi R)^2}}, \tag{13}$$

with n accounting for the number of helices wrapping around the fibre in one turn or per pitch P. From equation (13) we compute $L = 2.36$ nm. We note that there have been studies that consider deviations in the helices with respect to the axis of the cylinder, which equation (13) does not include [127]. The model for $\tilde{R} = 1.135$ predicts the correct number of helices per pitch $n = 5$ with the corresponding pitch angle $\Theta = 45.6°$. We find also agreement with 10% accuracy for the chiral structure of the strain $Pf1$ of the Inovirus phage, which has a different helical arrangement compared to the fd and $M13$ virions [109].

Another system considered is single-stranded DNA wrapped around carbon nanotubes. In aqueous solution it is shown to form helices with a pitch $P = 14$ nm [128]. Since the ssDNA backbone is 0.5 nm above the surface of the 0.8 nm diameter carbon nanotube, it is argued that the radius of the cylinder is $R = 0.9$ nm. From this we estimate $L = 5.24$ nm and the model correctly predicts a single wrapping helix ($n = 1$) with an axial angle of $\Theta = 22°$. Similarly, an example of two polysaccharide chains twining around a single-walled carbon nanotube with 1.5 nm diameter and an helical pitch $P = 10$ nm is reported [129]. For such a case, the radius $\tilde{R} = 0.35$ for which equation (2) has a minimum at $n = 2$, which is correct for the two chains winding around the nanotube. There are numerous other systems that display helical patterns that have not been considered with this model [130–135].

3. Conclusions

The ubiquitous nature of helical structures in low-dimensional systems observed in Nature is fascinating alone, yet the idea of chirality being Nature's sense of direction is even more intriguing. Although chirality is seen in many different energy landscapes from weak interacting particles in particle physics to the formation of our own hands, there has been no clear evidence of what the fundamental reasons are at the molecular level that gives rise to helical structures. Cylindrical surfaces offer the opportunity to study electrostatic interactions in the unique environment where one direction is very constrained due to the curvature, while the other is topologically flat extending out to large distances. With just a simple one-component plasma confined to a cylindrical surface the long-range nature of the electrostatic energy is able to go beyond breaking translational and rotational isometries, but also chiral (albeit with equal probability) isometry. Further investigations needs to be done to assess the universality of chiral arrangements coming out of electrostatic interactions.

We emphasize that many systems besides block copolymer melts are described with correlations that decay as $1/r$. These systems, including irradiated alloys [136, 137] and spatio-temporal patterns [136, 137], in the presence of competing interactions, generate patterns like those described in this paper. Spatio-temporal patterns with propagating fronts visualized in Taylor–Couette experiments and Rayleigh–Bérnard patterns in convection cells have long been studied [138]. In fact, block copolymer melts have shown pattern formation of a similar nature to those found in propagating fronts [137]. We expect these systems will develop similar chiral patterns to those discussed in this paper when confined to the surface of cylinders as others have seen with triblock copolymer assemblies that have displayed helical patterns [139, 56]. Further, we hope the chirality exhibited by the patterns formed on cylindrical surfaces in reaction–diffusion systems, such as those found in thermoreversible immiscible chains [140, 141], will be explored in the future.

Acknowledgments

The authors wish to thank S M Loverde, F J Solis and Y S Velichko for their help. MO acknowledges the NSF support award number DMR 0503943 for the initial studies that motivated this work. GV thanks the DOE grant DE-FG02-08ER46539 for financial support and KLK would like to thank the Krell Institute for their support with the CSGF award DE-FG02-97ER2530 from the DOE.

References

[1] Andelman D, Brochard F and Joanny J F 1987 *J. Chem. Phys.* **86** 3673–81
[2] Pettey D and Lubensky T C 1999 *Phys. Rev.* E **59** 1834–45
[3] Veatch S L and Keller S L 2003 *Biophys. J.* **85** 3074–83
[4] Liu J, Qi S A, Groves J T and Chakraborty A K 2005 *J. Phys. Chem.* B **109** 19960–9
[5] Hu Y F, Meleson K and Israelachvili J 2006 *Biophys. J.* **91** 444–53
[6] McConnell H M 2008 *ACS Chem. Biol.* **3** 265–7
[7] Messina R 2009 *J. Phys.: Condens. Matter* **21** 18
[8] Langmuir I 1933 *J. Chem. Phys.* **1** 756
[9] McConnell H M and Moy V T 1988 *J. Phys. Chem.* **92** 4520–5
[10] Lipp M M, Lee K Y C, Waring A and Zasadzinski J A 1997 *Biophys. J.* **72** 2783–804
[11] Wang S W, Poglitsch C L, Yatcilla M T, Robertson C R and Gast A P 1997 *Langmuir* **13** 5794–8
[12] McConnell H M 1989 *Proc. Natl Acad. Sci. USA* **86** 3452–5
[13] Stoycheva A D and Singer S J 2000 *Phys. Rev. Lett.* **84** 4657–60
[14] Seul M and Andelman D 1995 *Science* **267** 476–83
[15] Sagui C, Asciutto E and Roland C 2005 *Nano Lett.* **5** 389–95
[16] Netz R R, Andelman D and Schick M 1997 *Phys. Rev. Lett.* **79** 1058–61
[17] Kaganer V M, Mohwald H and Dutta P 1999 *Rev. Mod. Phys.* **71** 779–819
[18] Kosterlitz J M and Thouless D J 1973 *J. Phys. C: Solid State Phys.* **6** 1181–203
[19] Iwamoto M, Liu F and Ou-Yang Z C 2006 *J. Chem. Phys.* **125** 9
[20] Landau L D (ed) 1965 *Collected Papers* (New York: Gordon and Breach)

[21] Baus M 1980 *J. Stat. Phys.* **22** 111–9
[22] Mermin N D 1968 *Phys. Rev.* **176** 250
[23] Peierls R E 1936 *Helv. Phys. Acta* **7** (Suppl. II) 81
[24] Levin Y 2002 *Rep. Prog. Phys.* **65** 1577–632
[25] Mons S, Salesse C, Mioskowski C and Lebeau L 2002 *Chem. Phys. Lipids* **114** 99–102
[26] Stoycheva A D and Singer S J 2001 *Phys. Rev.* E **64** 13
[27] Stoycheva A D and Singer S J 2002 *Phys. Rev.* E **65** 15
[28] Imperio A and Reatto L 2006 *J. Chem. Phys.* **124** 10
[29] Honerkamp-Smith A R, Cicuta P, Collins M D, Veatch S L, den Nijs M, Schick M and Keller S L 2008 *Biophys. J.* **95** 236–46
[30] Wu T T, McCoy B M, Tracy C A and Barouch E 1976 *Phys. Rev.* B **13** 316–74
[31] Malescio G and Pellicane G 2004 *Phys. Rev.* E **70** 6
[32] Malescio G and Pellicane G 2003 *Nat. Mater.* **2** 97–100
[33] Glaser M A, Grason G M, Kamien R D, Kosmrlj A, Santangelo C D and Ziherl P 2007 *Europhys. Lett.* **78** 5
[34] Geissler M and Xia Y N 2004 *Adv. Mater.* **16** 1249–69
[35] Asciutto E, Roland C and Sagui C 2005 *Phys. Rev.* E **72** 15
[36] Pan A C, Garrahan J P and Chandler D 2005 *Phys. Rev.* E **72** 10
[37] Hedges L O, Jack R L, Garrahan J P and Chandler D 2009 *Science* **323** 1309–13
[38] Ballesta P, Duri A and Cipelletti L 2008 *Nat. Phys.* **4** 550–4
[39] Netz R R and Joanny J F 1999 *Macromolecules* **32** 9013–25
[40] de la Cruz M O 2008 *Soft Matter* **4** 1735–9
[41] Jagla E A 2004 *Phys. Rev.* E **70** 7
[42] Sayar M, de la Cruz M O and Stupp S I 2003 *Europhys. Lett.* **61** 334–40
[43] Weis R M and McConnell H M 1984 *Nature* **310** 47–9
[44] Singh A, Burke T G, Calvert J M, Georger J H, Herendeen B, Price R R, Schoen P E and Yager P 1988 *Chem. Phys. Lipids* **47** 135–48
[45] Sandler I M, Canright G S, Gao H J, Pang S J, Xue Z Q and Zhang Z Y 1998 *Phys. Rev.* E **58** 6015–26
[46] Nandi N and Vollhardt D 2002 *J. Phys. Chem.* B **106** 10144–9
[47] Kruger P and Losche M 2000 *Phys. Rev.* E **62** 7031–43
[48] Andelman D and Orland H 1993 *J. Am. Chem. Soc.* **115** 12322–9
[49] Kane S A 2002 *Langmuir* **18** 9853–8
[50] Benvegnu D J and McConnell H M 1992 *J. Phys. Chem.* **96** 6820–4
[51] Levin Y 2003 *J. Stat. Phys.* **110** 825–34
[52] Palmans A R A and Meijer E W 2007 *Angew. Chem. Int. Edn* **46** 8948–68
[53] Vera F, Serrano J L and Sierra T 2009 *Chem. Soc. Rev.* **38** 781–96
[54] Chappell J S and Yager P 1991 *Chem. Phys. Lipids* **58** 253–8
[55] Zhou Y and Shimizu T 2008 *Chem. Mater.* **20** 625–33
[56] Zhong S, Cui H G, Chen Z Y, Wooley K L and Pochan D J 2008 *Soft Matter* **4** 90–3
[57] Zerrouki D, Baudry J, Pine D, Chaikin P and Bibette J 2008 *Nature* **455** 380–2
[58] Wu Y Y, Cheng G S, Katsov K, Sides S W, Wang J F, Tang J, Fredrickson G H, Moskovits M and Stucky G D 2004 *Nat. Mater.* **3** 816–22
[59] Valery C, Paternostre M, Robert B, Gulik-Krzywicki T, Narayanan T, Dedieu J C, Keller G, Torres M L, Cherif-Cheikh R, Calvo P and Artzner F 2003 *Proc. Natl Acad. Sci. USA* **100** 10258–62
[60] Spector M S, Selinger J V, Singh A, Rodriguez J M, Price R R and Schnur J M 1998 *Langmuir* **14** 3493–500
[61] Selinger J V, MacKintosh F C and Schnur J M 1996 *Phys. Rev.* E **53** 3804–18
[62] Schnur J M 1993 *Science* **262** 1669–76
[63] Pickett G T, Gross M and Okuyama H 2000 *Phys. Rev. Lett.* **85** 3652–5
[64] Kohlstedt K L, Solis F J, Vernizzi G and de la Cruz M O 2007 *Phys. Rev. Lett.* **99** 4
[65] Grason G M and Bruinsma R F 2007 *Phys. Rev.* E **76** 17
[66] Weis J J 2003 *J. Phys.: Condens. Matter* **15** S1471–95
[67] Iwamoto M and Zhong-can O Y 2004 *Phys. Rev. Lett.* **93** 4
[68] Hurley M M and Singer S J 1992 *J. Phys. Chem.* **96** 1938–50
[69] Hu Y F and Israelachvili J 2008 *Colloids Surf.* B **62** 22–30
[70] Stottrup B L, Veatch S L and Keller S L 2004 *Biophys. J.* **86** 2942–50
[71] Wang J, Caffrey M, Bedzyk M J and Penner T L 1994 *J. Phys. Chem.* **98** 10957–68
[72] Zasadzinski J A, Viswanathan R, Madsen L, Garnaes J and Schwartz D K 1994 *Science* **263** 1726–33
[73] Solis F J, Stupp S I and de la Cruz M O 2005 *J. Chem. Phys.* **122** 9
[74] Naydenov A, Pincus P A and Safran S A 2007 *Langmuir* **23** 12016–23
[75] Spurlin T A and Gewirth A A 2007 *J. Am. Chem. Soc.* **129** 11906
[76] Kaler E W, Herrington K L, Murthy A K and Zasadzinski J A N 1992 *J. Phys. Chem.* **96** 6698–707
[77] Cheng H and de la Cruz M O 2003 *J. Chem. Phys.* **119** 12635–44
[78] Liu J F and Ducker W A 1999 *J. Phys. Chem.* B **103** 8558–67
[79] Folkers J P, Laibinis P E, Whitesides G M and Deutch J 1994 *J. Phys. Chem.* **98** 563–71
[80] Meyer E E, Lin Q, Hassenkam T, Oroudjev E and Israelachvili J N 2005 *Proc. Natl Acad. Sci. USA* **102** 6839–42
[81] Dobrynin A V, Deshkovski A and Rubinstein M 2000 *Phys. Rev. Lett.* **84** 3101–4
[82] Cheng H and de la Cruz M O 2006 *Macromolecules* **39** 1961–70
[83] Dobrynin A V 2008 *Curr. Opin. Colloid Interface Sci.* **13** 376–88
[84] Lobaskin V and Netz R R 2007 *Europhys. Lett.* **77** 5
[85] Flory P 1971 *Principles of Polymer Chemistry* (Ithaca, NY: Cornell University Press)
[86] Loverde S M, Solis F J and de la Cruz M O 2007 *Phys. Rev. Lett.* **98** 4
[87] Loverde S M, Velichko Y S and de la Cruz M O 2006 *J. Chem. Phys.* **124** 7
[88] González-Mozuelos P and de la Cruz M O 1994 *J. Chem. Phys.* **100** 507–17
[89] Limbach H J, Arnold A, Mann B A and Holm C 2006 *Comput. Phys. Commun.* **174** 704–27
[90] Levin Y and Dawson K A 1990 *Phys. Rev.* A **42** 1976–81
[91] de la Cruz M O 1991 *Phys. Rev. Lett.* **67** 85–8
[92] Tsori Y, Andelman D and Schick M 2000 *Phys. Rev.* E **61** 2848–58
[93] Pini D, Ge J L, Parola A and Reatto L 2000 *Chem. Phys. Lett.* **327** 209–15
[94] Ma W L, Yang C Y, Gong X, Lee K and Heeger A J 2005 *Adv. Funct. Mater.* **15** 1617–22
[95] Van Workum K and Douglas J F 2006 *Phys. Rev.* E **73** 17
[96] Yamamoto T, Manaka T and Iwamoto M 2007 *J. Chem. Phys.* **126** 17
[97] Deutsch J M and Goldenfeld N D 1982 *J. Physique* **43** 651–4
[98] Deng Y J and Blote H W J 2002 *Phys. Rev. Lett.* **88** 4
[99] Lehn J M 1988 *Angew. Chem. Int. Edn* **27** 89–112
[100] Vernizzi G and de la Cruz M O 2007 *Proc. Natl Acad. Sci. USA* **104** 18382–6
[101] Lim M M D, Velichko Y S, de la Cruz M O and Vernizzi G 2008 *J. Phys. Chem.* B **112** 5423–7
[102] Bowick M J, Cacciuto A, Nelson D R and Travesset A 2006 *Phys. Rev.* B **73** 16
[103] Endo I and Koibuchi H 2006 *Phys. Lett.* A **350** 11–6
[104] Velichko Y S and de la Cruz M O 2005 *Phys. Rev.* E **72** 4
[105] Kohlstedt K L, Vernizzi G and de la Cruz M O 2009 *Phys. Rev.* E submitted
[106] Gomez J, Sagues F and Reigada R 2008 *Phys. Rev.* E **77** 5

[107] Tombolato F, Ferrarini A and Grelet E 2006 *Phys. Rev. Lett.* **96** 4
[108] Marvin D A, Welsh L C, Symmons M F, Scott W R P and Straus S K 2006 *J. Mol. Biol.* **355** 294–309
[109] Thiriot D S, Nevzorov A A, Zagyanskiy L, Wu C H and Opella S J 2004 *J. Mol. Biol.* **341** 869–79
[110] Claessens M, Semmrich C, Ramos L and Bausch A R 2008 *Proc. Natl Acad. Sci. USA* **105** 8819–22
[111] Vernizzi G, Kohlstedt K L and de la Cruz M O 2009 *Soft Matter* **5** 736–9
[112] Straus S K, Scott W R P and Marvin D A 2008 *Eur. Biophys. J. Biophys. Lett.* **37** 1077–82
[113] Harris A B, Kamien R D and Lubensky T C 1999 *Rev. Mod. Phys.* **71** 1745–57
[114] Selinger R L B, Selinger J V, Malanoski A P and Schnur J M 2004 *Phys. Rev. Lett.* **93** 4
[115] Erb R M, Son H S, Samanta B, Rotello V M and Yellen B B 2009 *Nature* **457** 999–1002
[116] Yin Y D and Xia Y N 2003 *J. Am. Chem. Soc.* **125** 2048–9
[117] Levin Y, Trizac E and Bocquet L 2003 On the fluid–fluid phase separation in charged-stabilized colloidal suspensions *Workshop on Effective Many-Body Interactions and Correlations in Soft Matter* (Lyon: Institute of Physics Publishing) pp S3523–36
[118] Kondo Y and Takayanagi K 2000 *Science* **289** 606–8
[119] Hunyadi V, Chretien D, Flyvbjerg H and Janosi I M 2007 *Biol. Cell* **99** 117–28
[120] Israelachvili J 1994 *Langmuir* **10** 3774–81
[121] Jiang H Z, Guler M O and Stupp S I 2007 *Soft Matter* **3** 454–62
[122] Palmer L C and Stupp S I 2008 *Acc. Chem. Res.* **41** 1674–84
[123] Lorieau J L, Day L A and McDermott A E 2008 *Proc. Natl Acad. Sci. USA* **105** 10366–71
[124] Marvin D A, Hale R D, Nave C and Citterich M H 1994 *J. Mol. Biol.* **235** 260–86
[125] Dogic Z and Fraden S 2000 *Langmuir* **16** 7820–4
[126] Grelet E and Fraden S 2003 *Phys. Rev. Lett.* **90** 4
[127] Overman S A, Tsuboi M and Thomas G J 1996 *J. Mol. Biol.* **259** 331–6
[128] Campbell J F, Tessmer I, Thorp H H and Erie D A 2008 *J. Am. Chem. Soc.* **130** 10648–55
[129] Numata M, Asai M, Kaneko K, Bae A H, Hasegawa T, Sakurai K and Shinkai S 2005 *J. Am. Chem. Soc.* **127** 5875–84
[130] Kumaki J, Sakurai S and Yashima E 2009 *Chem. Soc. Rev.* **38** 737–46
[131] Oda R, Artzner F, Laguerre M and Huc I 2008 *J. Am. Chem. Soc.* **130** 14705–12
[132] Chappell J S and Yager P 1991 *Chem. Phys.* **150** 73–9
[133] Berthier D, Buffeteau T, Leger J M, Oda R and Huc I 2002 *J. Am. Chem. Soc.* **124** 13486–94
[134] Kanduc M, Dobnikar J and Podgornik R 2009 *Soft Matter* **5** 868–77
[135] Brizard A, Oda R and Huc I 2005 *Low Molecular Mass Gelators: Design, Self-Assembly, Function* (Berlin: Springer) pp 167–218
[136] Enrique R A and Bellon P 2000 *Phys. Rev. Lett.* **84** 2885–8
[137] Liu F and Goldenfeld N 1989 *Phys. Rev.* A **39** 4805–10
[138] van Saarloos W 2003 *Phys. Rep.-Rev. Sec. Phys. Lett.* **386** 29–222
[139] Jinnai H, Kaneko T, Matsunaga K, Abetz C and Abetz V 2009 *Soft Matter* **5** 2042–6
[140] Glotzer S C, Dimarzio E A and Muthukumar M 1995 *Phys. Rev. Lett.* **74** 2034–7
[141] Tran-Cong Q and Harada A 1996 *Phys. Rev. Lett.* **76** 1162–5